



Amplitude normalized imaging condition for separated wavefields

Alba Ordoñez, EOST/PGS, and Walter Söllner *, PGS

Copyright 2013, SBGf - Sociedade Brasileira de Geofísica

This paper was prepared for presentation during the 13th International Congress of the Brazilian Geophysical Society held in Rio de Janeiro, Brazil, August 26-29, 2013.

Contents of this paper were reviewed by the Technical Committee of the 13th International Congress of the Brazilian Geophysical Society and do not necessarily represent any position of the SBGf, its officers or members. Electronic reproduction or storage of any part of this paper for commercial purposes without the written consent of the Brazilian Geophysical Society is prohibited.

Abstract

The imaging condition needs special attention in imaging of separated wavefields because of the increased complexity of the source wavefield. Starting from reciprocity relations and using an amplitude normalized wavefield decomposition, we introduce a new deconvolution imaging condition: the subsurface image is determined from the upgoing pressure and the downgoing vertical particle velocity wavefields.

In a recent work, Lameloise et al. (2012) elaborated on migration of separated wavefields using dual-sensor towed streamer data of a simultaneous source system. This work was the starting point to set up a feasibility study and test the new imaging condition. Synthetic and real data examples showed that this approach leads to a better match between the depth images of multiples and primaries.

Introduction

Conform Claerbout's principle (Claerbout, 1971), at any subsurface level the image I is derived from the source and receiver wavefields by taking the subset of the impulse reflection response which corresponds to the zero-offset scattered field estimated at zero-time. The source wavefield originated at the seismic source is forward propagated into the subsurface reaching the medium discontinuities. The receiver wavefield, generated at the subsurface discontinuities and measured at the receiver level is backward propagated into the subsurface. The depth image I is given by the division in the frequency-space domain of the receiver (upgoing) wavefield by the source (downgoing) wavefield, integrated over frequencies. This may be expressed by (Claerbout, 1971):

$$I(\mathbf{x}) = \int_{\omega} \frac{\text{Upgoing wavefield}}{\text{Downgoing wavefield}} d\omega \quad (1)$$

where \mathbf{x} corresponds to the image position and ω is the angular frequency. Following this principle, it is possible to properly collapse primary reflections into the image.

This paper deals with migration of separated wavefields using dual-sensor towed streamer data of a simultaneous source system. In separated wavefield imaging, the

upgoing (receiver) wavefield and the downgoing (source) wavefield contain primaries and multiples and the imaging condition needs to be accordingly adapted. Three different imaging conditions based on Claerbout's principle (Equation 1) will be evaluated, as well as their capability of recovering a proper image of primaries and multiples.

Method

One possible method to estimate the reflection response at any level is to employ reciprocity in two different states of an acoustic model (Fokkema and van den Berg, 1993; Amundsen, 2001).

Considering the sea surface above the active source and the sea bottom below the towed streamer, two different states of an acoustic model are defined and illustrated in Figure 1.

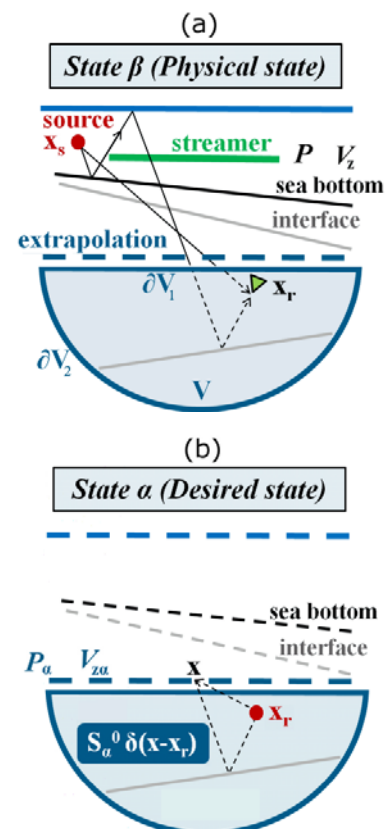


Figure 1: Representation of the two states β (a) and α (b).

On one hand, state β (Figure 1 a) refers to the physical seismic experiment where the source is identified by its position \mathbf{x}_s . An extrapolation level of separated wavefields is set to simulate data (P and V_z) recorded at a virtual receiver position \mathbf{x}_r , just below the extrapolation level. A volume V is considered enclosed by a surface characterized by a flat top boundary (∂V_1) chosen at the extrapolation level and a hemisphere of infinite radius (∂V_2). The acoustic properties of this model match the medium parameters within and outside V . In this situation, surface multiples are generated at the sea surface and internal multiples at the overburden reflectors.

On the other hand, state α (Figure 1 b) corresponds to the desired state. Wavefields (P_α and $V_{z\alpha}$) are generated by a monopole point source located at \mathbf{x}_r and recorded by a virtual receiver at the position \mathbf{x} of the separation level. We define the same volume V as for state β . However, in this case the free surface is absent and the overburden is continuously non-reflective.

At the extrapolation level we separate the wavefield in upgoing and downgoing components. The separation may be performed using amplitude normalization for the pressure wavefield output, in which case the total pressure wavefield, $P = U^{(P)} + D^{(P)}$, is expressed by the addition of the upgoing $U^{(P)}$ and the downgoing $D^{(P)}$ pressure components. Or it may be performed using amplitude normalization for the vertical velocity wavefield output, in this case the total velocity wavefield, $V_z = U^{(V_z)} + D^{(V_z)}$, is expressed by the sum of the upgoing $U^{(V_z)}$ and the downgoing $D^{(V_z)}$ vertical velocity components. Here, we will make use also of the flux normalization (Ursin, 1984), in which case the total pressure wavefield, $P = \sqrt{\frac{\rho\omega}{2b}}(U + D)$, and the total vertical velocity, $V_z = \sqrt{\frac{b}{2\rho\omega}}(-U + D)$, are expressed by the upgoing U and downgoing D flux components as well as the material density ρ at the separation level, the circular frequency ω , the medium velocity c , and the differential operator $b = \sqrt{\frac{\omega^2}{c^2} + \partial^2 x + \partial^2 y}$.

In a small source-free depth interval around the extrapolation level at ∂V_1 we make use of the amplitude normalized wavefield separation to derive the wavefield identity (Wapenaar and Berkhout, 1989) for the pressure and vertical velocity wavefields, $\int_{\partial V_1} (P_\alpha V_z - V_{z\alpha} P) dS = 2\partial N1 U_\alpha P D(V_z) + D_\alpha P U(V_z) dS$. A similar identity may also be found for the flux normalized wavefield decomposition (Wapenaar et al., 2008) $\int_{\partial V_1} (P_\alpha V_z - V_{z\alpha} P) dS = \partial N1 U_\alpha D - U D_\alpha dS$.

By setting up reciprocity relations between the two states and using amplitude normalized wavefield decomposition, an integral equation in the frequency-space domain gives the desired reflected pressure (P_α^{refl}) in terms of the upgoing pressure ($U^{(P)}$), the downgoing vertical particle velocity ($D^{(V_z)}$), the complex $i\omega$ and the source

contribution of the desired state (S_α^0). This integral equation writes:

$$2i\omega \int_{\partial V_1} P_\alpha^{refl}(\mathbf{x}_r, \mathbf{x}) D^{(V_z)}(\mathbf{x}, \mathbf{x}_s) dS = -S_\alpha^0 U^{(P)}(\mathbf{x}_r, \mathbf{x}_s) \quad (2)$$

Thereafter, assuming sufficient available data, an inversion at any image level gives the needed reflection response for extracting the subsurface image. Note, in the derivation of Equation 2, we also applied to the desired pressure (P_α) source-receiver reciprocity, which interchanged virtual source and receiver positions. A similar integral equation could be found for flux normalized separated wavefields:

$$i\omega \int_{\partial V_1} U_\alpha^{refl}(\mathbf{x}_r, \mathbf{x}) D(\mathbf{x}, \mathbf{x}_s) dS = -\sqrt{\frac{\rho\omega}{2b}} S_\alpha^0 U(\mathbf{x}_r, \mathbf{x}_s) \quad (3)$$

Based on Equation 2, we will define now two different imaging conditions for separated wavefields using Claerbout's imaging principle (Equation 1). We will also present a third imaging condition based on Equation 3.

Ignoring the overburden related crosstalk for now, we follow Claerbout's principle in common source gather and extract from Equation 2, the depth images of primaries and multiples assuming zero-time and coincident virtual source-receiver positions at the image level ($\mathbf{x} = \mathbf{x}_r$).

These depth images correspond to the impulse reflection response: $\frac{P_\alpha^{refl}}{S_\alpha^0}$. For a single shot fired at position \mathbf{x}_s and for each frequency value, the integrand appearing in Equation 2 reduces to a constant. Sum over frequencies is used to satisfy the zero-lag condition. As in practice multiple shot gathers are available, the data is migrated sequentially and stacked over all source positions. Then, we can define:

$$I(\mathbf{x}) = \sum_{\mathbf{x}_s} \sum_{\omega} \frac{U^{(P)}(\mathbf{x} = \mathbf{x}_r, \omega; \mathbf{x}_s) D_f^{(V_z)*}(\mathbf{x} = \mathbf{x}_r, \omega; \mathbf{x}_s)}{\langle D_f^{(V_z)}(\mathbf{x} = \mathbf{x}_r, \omega; \mathbf{x}_s) D_f^{(V_z)*}(\mathbf{x} = \mathbf{x}_r, \omega; \mathbf{x}_s) \rangle + \varepsilon^2} \quad (4)$$

where $D_f^{(V_z)} = -2i\omega D^{(V_z)}$. To avoid numerical instabilities, we multiplied the numerator and denominator by the complex conjugate downgoing wavefield, considered a smoothing operator denoted by $\langle \rangle$ and added a constant ε^2 .

In this paper, we will migrate data using Equation 4 and we will also test an imaging condition which defines the source wavefield as the downgoing part of the vertical particle velocity (without filtering by $-i\omega$), as illustrated below:

$$I(\mathbf{x}) = \sum_{\mathbf{x}_s} \sum_{\omega} \frac{U^{(P)}(\mathbf{x} = \mathbf{x}_r, \omega; \mathbf{x}_s) D^{(V_z)*}(\mathbf{x} = \mathbf{x}_r, \omega; \mathbf{x}_s)}{\langle D^{(V_z)}(\mathbf{x} = \mathbf{x}_r, \omega; \mathbf{x}_s) D^{(V_z)*}(\mathbf{x} = \mathbf{x}_r, \omega; \mathbf{x}_s) \rangle + \varepsilon^2} \quad (5)$$

Subsurface images resulting from Equations 4 and 5 will be compared with the ones obtained by an imaging

condition previously used by Whitmore et al. (2010) and Lameloise et al. (2012):

$$I(\mathbf{x}) = \sum_{\mathbf{x}_s} \sum_{\omega} \frac{U^{(P)}(\mathbf{x} = \mathbf{x}_r, \omega; \mathbf{x}_s) D^{(P)*}(\mathbf{x} = \mathbf{x}_r, \omega; \mathbf{x}_s)}{\langle D^{(P)}(\mathbf{x} = \mathbf{x}_r, \omega; \mathbf{x}_s) D^{(P)*}(\mathbf{x} = \mathbf{x}_r, \omega; \mathbf{x}_s) \rangle + \epsilon^2} \quad (6)$$

While Equations 4 and 5 follows from the amplitude normalized wavefield decomposition, Equation 6 follows from the flux normalized wavefield decomposition.

Synthetic data example

To evaluate the defined imaging conditions, we considered a model formed by a layer of water, five embedded diffractors, and a free surface top boundary. In order to generate pressure and vertical particle velocity wavefields of a dual simultaneous source system, we simulated two typical seismic sources fired with a time delay of 500 ms, at the same horizontal position and at the distinct depths of 10 and 14 m.

After decomposing seismic wavefields into up and downgoing components at a predefined horizontal level, wavefields are downward extrapolated and combined using the three different imaging conditions (Figure 2).

To image multiples (Figures 2 a, d, g), the complete downgoing wavefield which includes multiple reflections from the free surface (without the direct wave) is considered as source wavefield, whereas to migrate primaries (Figures 2 b, e, h) the direct wavefield is used as source. As for the receiver wavefield, it corresponds to the upgoing pressure, computed from wavefield separation of the scattered pressure and the vertical particle velocity. The diffractors are clearly discernible by applying Equations 4 and 5 (Figures 2 a, b, d, e). In this case, the vertical resolution is better than employing Equation 6 (Figures 2 g, h), which gives an image with oscillations in depth and stronger crosstalk effects. Besides, employing Equations 4 and 5 leads to a perfect match between the spectra of multiples and primaries depth images (Figures 2 c, f), which is not the case when using Equation 6 (Figure 2 i).

Field data example

A seismic survey was operated in the Norwegian Sea using dual-sensor towed streamers of a dual simultaneous source system (Parkes and Hegna, 2011). Depth images and spectra of multiples and primaries derived from Equations 4 and 5 are compared with migration results obtained with Equation 6.

Applying the obliquity scaling and the frequency filter in the imaging condition of Equation 4 leads to a proper match of the images and spectra of the migrated multiples and primaries (Figure 3). However, due to the smaller angle distribution of multiple reflections compared to primaries, this match is less accurate when using the two other imaging conditions (Figures 4 and 5). Some observed differences could also be related to the higher sensitivity of primaries to the velocity model.

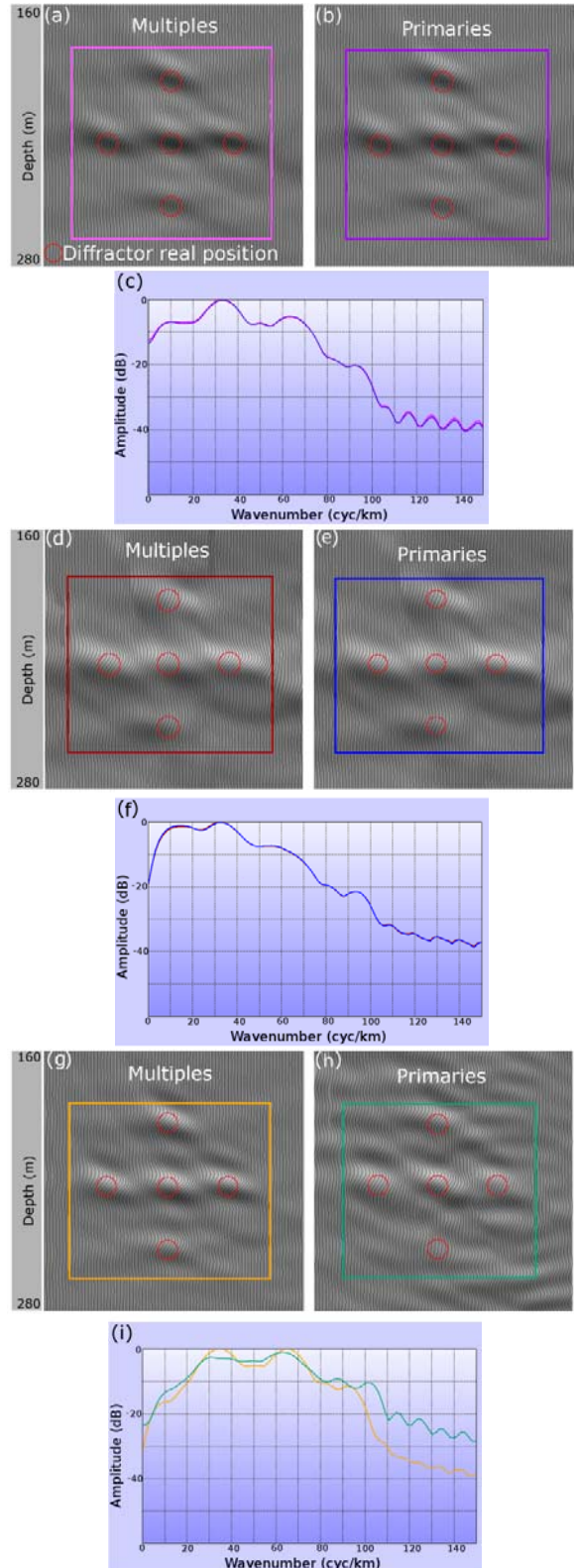


Figure 2: Depth images obtained from one dual simultaneous source record with Equations 4 (a-b), 5 (d-e) and 6 (g-h) and spectral comparison of the marked windows (c, f, i).

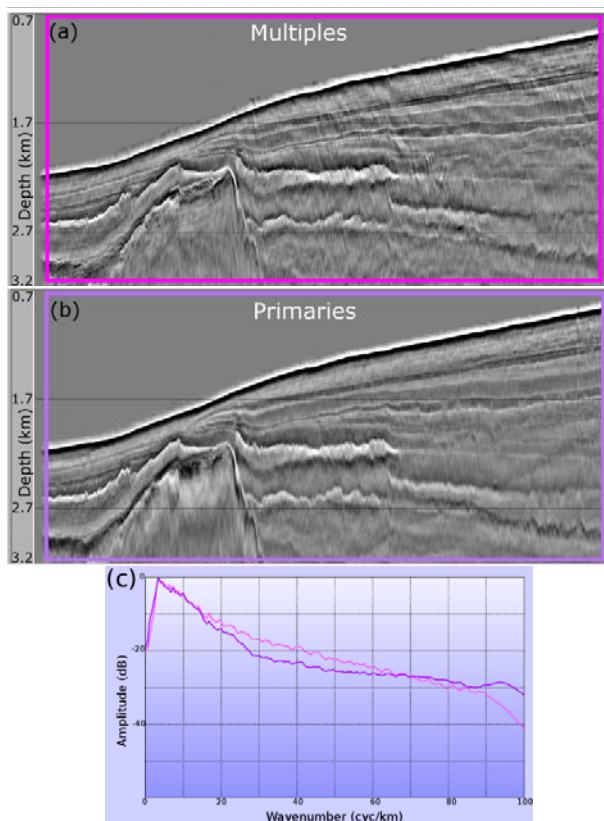


Figure 3: Images (a-b) and spectra (c) using Equation 4.

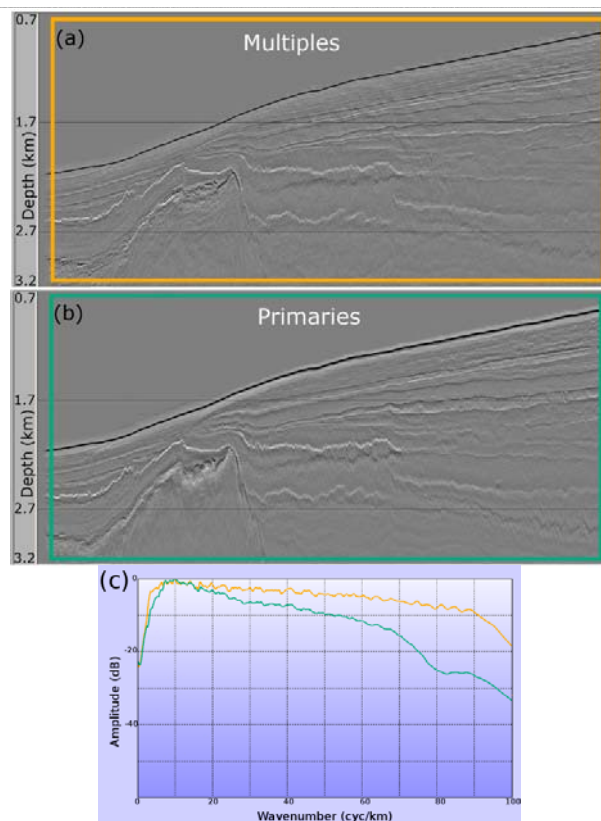


Figure 5: Images (a-b) and spectra (c) using Equation 6.

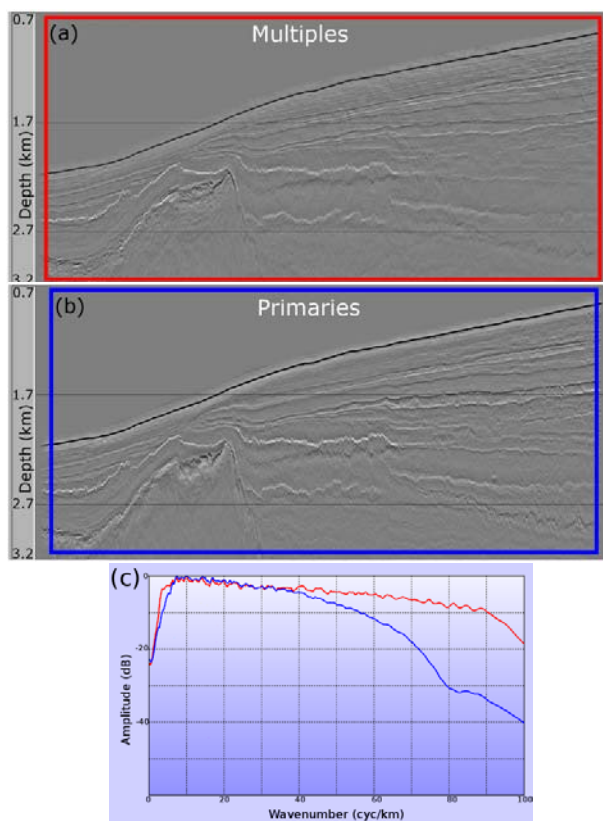


Figure 4: Images (a-b) and spectra (c) using Equation 5.

Conclusions

Starting from reciprocity relations, the subsurface reflectivity is derived from an integral equation inversion at the image level. The integral equation contains the upgoing pressure, the downgoing vertical particle velocity and a $-i\omega$ filter. By considering Claerbout's principle, we defined a new deconvolution imaging condition which includes an obliquity scaling and a frequency filter. Through synthetic and real data examples, we tested and compared it to a previously used imaging condition. The new imaging condition resulted in a better match between the depth images of multiples and primaries.

References

Amundsen, L., 2001, Elimination of the free-surface related multiples without need of the source wavelet: *Geophysics*, 66, 327-341.

Claerbout, J.F., 1971, Toward a unified theory of reflector mapping: *Geophysics*, 36, 467-481.

Fokkema, J.T., and P.M. van den Berg, 1993, *Seismic applications of acoustic reciprocity*: Elsevier Science.

Lameloise, C., Söllner, W., Hegna, S., and N.D. Whitmore, 2012, Broadband Depth Imaging from Separated Wavefields: 74th EAGE Conference & Exhibition, Extended Abstract, X047.

Parkes, G., and S. Hegna, 2011, An acquisition system that extracts the earth response from seismic data: *First Break*, 29, 81-87.

Ursin, B., 1983, Review of elastic and electromagnetic wave propagation in horizontally layered media: *Geophysics*, 48, 1063-1081.

Wapenaar, K., and A.J. Berkhout, 1989, *Elastic wavefield extrapolation*: Elsevier Science.

Wapenaar, K., Slob, E., and R. Snieder, 2008, Seismic and electromagnetic controlled-source interferometry in dissipative media: *Geophysical Prospecting*, 56, 419-434.

Whitmore, N.D., Valenciano, A.A., Söllner, W., and S. Lu, 2010, Imaging of primaries and multiples using a dual-sensor towed streamer: 80th Annual International Meeting, SEG, Extended Abstract, 3187-3192.

Acknowledgments

We thank PGS for permission to present this work and Charles Lameloise for his contribution.